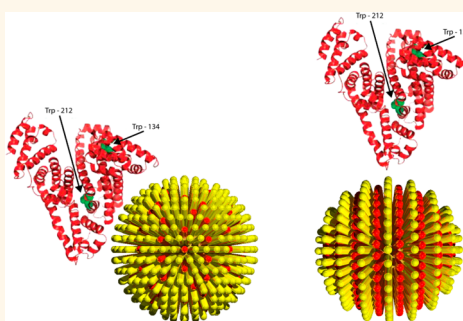


Effects of Surface Compositional and Structural Heterogeneity on Nanoparticle–Protein Interactions: Different Protein Configurations

Rixiang Huang,[†] Randy P. Carney,[‡] Kaoru Ikuma,[§] Francesco Stellacci,[‡] and Boris L. T. Lau^{§,*}

[†]Department of Geology, Baylor University, One Bear Place #97354 Waco, Texas 76798, United States, [‡]Institute of Materials, École Polytechnique Fédérale de Lausanne, Lausanne 1015, Switzerland, and [§]Department of Civil and Environmental Engineering, University of Massachusetts Amherst, 18B Marston Hall, 130 Natural Resources Road, Amherst, Massachusetts 01003, United States

ABSTRACT As nanoparticles (NPs) enter into biological systems, they are immediately exposed to a variety and concentration of proteins. The physicochemical interactions between proteins and NPs are influenced by the surface properties of the NPs. To identify the effects of NP surface heterogeneity, the interactions between bovine serum albumin (BSA) and gold NPs (AuNPs) with similar chemical composition but different surface structures were investigated. Different interaction modes and BSA conformations were studied by dynamic light scattering, circular dichroism spectroscopy, fluorescence quenching and isothermal titration calorimetry (ITC). Depending on the surface structure of AuNPs, BSA seems to adopt either a “side-on” or an “end-on” conformation on AuNPs. ITC demonstrated that the adsorption of BSA onto AuNPs with randomly distributed polar and nonpolar groups was primarily driven by electrostatic interaction, and all BSA were adsorbed in the same process. The adsorption of BSA onto AuNPs covered with alternating domains of polar and nonpolar groups was a combination of different interactions. Overall, the results of this study point to the potential for utilizing nanoscale manipulation of NP surfaces to control the resulting NP–protein interactions.



KEYWORDS: protein conformation · surface heterogeneity · bovine serum albumin · gold nanoparticles · bionano interface

The interaction between nanoparticles (NPs) and proteins is a topic of high relevance for the medical application of nanomaterials.^{1,2} As NPs enter into biological systems, they are exposed to a wide range of proteins of different amounts, and it is the NP–protein complexes rather than the NPs alone that determine the resulting biological responses.³ Understanding the nature of interactions (*e.g.*, interaction forces, binding sites, and affinity) and the subsequent effects (*e.g.*, conformation and activity of the interacting proteins, stability and functionality of the NPs) are crucial for better design and handling of nanomaterials in a biological environment.

It has been shown that proteins can bind specifically or nonspecifically to NPs suspended in a biological fluid⁴ to form a tightly bound, yet dynamic surface coating known as the “protein corona”. This corona

largely determines the reactivity and functionality of NPs, thus serving as the biological identity of the nanomaterials.⁵ The initial adsorption and subsequent exchange of proteins in the corona change over time as a function of the affinity of the proteins for the NP. The composition of protein corona is dependent on the NP size,⁶ shape,⁷ and surface properties such as chemical composition,⁸ surface charge,⁹ and surface hydrophobicity.¹⁰ The mono- or bilayer of proteins formed on the NP surfaces is often described as the “hard corona” due to the slow time scale of protein exchange and strong binding energies associated with the complex.¹¹ Following protein adsorption, this corona is “read” by the cellular surface machinery to direct subsequent NP–cell interactions.³ Ultimately, the long-lived hard protein corona has been found to determine the fate of the NPs upon transfer

* Address correspondence to borislau@engin.umass.edu.

Received for review April 5, 2013 and accepted May 30, 2014.

Published online May 30, 2014
10.1021/nn501203k

© 2014 American Chemical Society

between biological fluids (e.g., plasma, cytoplasm).¹² As such, targeted NP usage could be improved by manipulating the surface properties of NPs to bind proteins selectively.^{4,13} One such modification could be done by introducing different forms of heterogeneity on the NP surface.¹⁴ Although numerous studies have investigated the effects of surface properties on protein adsorption, most of them were done using NPs with a homogeneous surface and few have targeted the influence of surface heterogeneity within a given NP surface.^{15,16} Little is known about how NP surface heterogeneity at the nanoscale (which is comparable to the size of proteins) affects the adsorption of proteins and the resulting protein coating on NPs.

Gold NPs (AuNPs) synthesized with a binary mixture of hydrophobic and hydrophilic thiolated ligand molecules have been shown to form a ligand shell with stripe-like domains of alternating hydrophobic/hydrophilic composition.^{17–19} These stripe-like domains have a characteristic thickness on the order of a single nanometer, leading to surface heterogeneities at similar scales as those found on proteins. This unique structure has been shown to possess interesting properties regarding wettability,²⁰ interfacial energy²¹ and cell membrane penetration.¹⁹ For example, only those particles with striped ligand shells were shown to penetrate cell membranes in an energy-independent way, while particles with a random arrangement of ligand in their ligand shell enter cells through energy-dependent pathways. These NPs also have different spatial distribution/localization within cells. These observations suggest that the different interactions with biomolecules due to NP surface heterogeneity may be responsible for their different behaviors in cellular uptake. By further understanding the effect of NP surface heterogeneity on NP–biomolecule interactions and the underlying mechanisms, we may (1) improve the design of NPs (by adding surface heterogeneity as a new tunable property) for specific biological applications and (2) better predict their fate and transport in biological systems.

In our previous work, the influence of NP surface heterogeneity was found to be dependent on the dimension of surface features on NPs and proteins.²² We focused this present study on the adsorption of BSA (which has comparable size to the NPs used) on two types of NPs. All NPs used were nearly identical in shape, size, and composition but different only in the ligand shell morphology. In these particles, the NP surface heterogeneity was observed in the form of two ligands being randomly distributed or forming alternating stripe-like domains on the surface of each NP. By using AuNPs with similar surface heterogeneity features but different charged functional groups (*i.e.*, with $-\text{COO}^-$ or $-\text{SO}_3^-$ terminals), we confirmed that the observed protein adsorption behavior was dependent on NP structural heterogeneity and independent

of particular polar groups. We further characterized the interactions of the AuNPs with a mixture of two proteins to test the NP surface heterogeneity effects in a more complex environment.


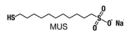
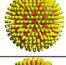
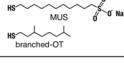
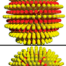
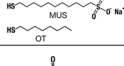
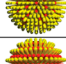
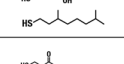
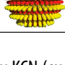
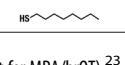
A combination of dynamic light scattering (DLS), circular dichroism (CD) spectroscopy, fluorescence quenching and isothermal titration calorimetry (ITC) was applied to characterize the interactions between proteins and AuNPs. DLS was used to monitor the increases in AuNP size due to self-aggregation or protein adsorption. CD spectroscopy characterized the secondary structure of the adsorbed BSA. Fluorescence quenching revealed the possible binding sites by quantifying the quenching of fluorescence from certain chromophores in the BSA structure by AuNP adsorption. ITC characterized the underlying thermodynamics of the interaction. Results from individual techniques were collectively examined to understand the mechanisms of interaction.

RESULTS AND DISCUSSION

Characteristics of the AuNPs. Two types of AuNPs were used in this study. The MUS-type AuNPs were coated with either (1) all negatively charged, sulfonated alkanethiols (11-mercapto-1-undecanesulfonate, MUS); (2) a 2:1 molar mixture of MUS and 1-octanethiol (OT) (now referred to as MUS/OT); or (3) a 2:1 molar mixture of MUS and a branched version of OT (3,7 dimethyl octane 1-thiol, brOT) (MUS/brOT). The MPA-type AuNPs were MPA/brOT and MPA/OT, resembling MUS/brOT and MUS/OT in their surface organizations of the coating ligands, with the negatively-charged MUS substituted with mercaptopropionic acid (MPA). The synthesis and characterization of these AuNPs have been performed in previous studies^{17–19} (details are also available in the Supporting Information). To ensure the uniformity of particle size and shape, the AuNPs were characterized by TEM and DLS before use. TEM showed that the AuNPs were mostly spherical and slightly angular. The size distributions of the two types of AuNPs based on TEM image analysis can be found in Figure S1 (Supporting Information). The physical and chemical characteristics of the two types of AuNPs were presented in Table 1. TEM revealed that the three MUS-type AuNPs are similar in size. The sizes of the two MPA-type AuNPs are similar to each other but slightly larger (by ~ 1 nm) in core diameter than the MUS-type AuNPs.

As shown in previous studies using scanning tunneling microscopy, depending on the types of self-assembled monolayer (SAM), the polar and nonpolar ligands can be randomly distributed or form alternating stripes on the surface of AuNPs.^{17,18} The combination of MUS and brOT forms a surface with randomly distributed ligands. The combination of MUS (or MPA) and OT leads to alternating polar and nonpolar stripes, and the dimension of the stripes is dependent on the ratio of the MUS (or MPA) to OT. The headgroup

TABLE 1. Physical and Chemical Properties of the Two Types of AuNPs Used in This Study

Nanoparticles	Ligand Shell composition*	Ligand shell morphology and chemical structures	Core size, $D_{TEM}^{\#}$ (nm)	Hydrodynamic diameter, D_h^{\S} (nm)
MUS	100% MUS	 	4.5±1.1	10.8±0.2
MUS/brOT	66% MUS 34% brOT	 	4.7±0.9	12.5±2.4
MUS/OT	66% MUS 34% OT	 	3.9±0.8	9.4±1.0
MPA/brOT	66% MPA 34% brOT	 	5.8±0.3	10.6±0.4
MPA/OT	66% MPA 34% OT	 	5.7±0.3	9.9±0.5

* Based on ^1H NMR analysis of ligands after gold core decomposition by KCN (except for MPA/brOT).²³ $^{\#}$ Determined from TEM images and expressed as average diameter \pm standard deviation. § Determined by DLS with a fixed detector angle of 173° based on volume-based size distribution.

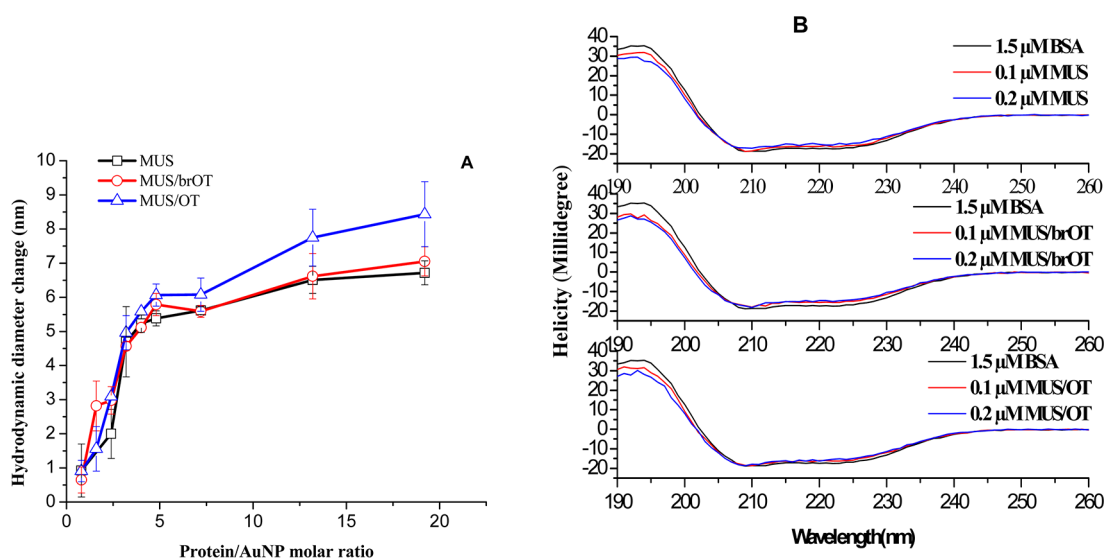


Figure 1. (A) ΔD_h of MUS-type AuNPs due to the adsorption of BSA. BSA concentration was kept at 0.05 μM in 10 mM 7.4 sodium phosphate buffer with varying amounts of AuNPs added. Error bars represent the standard deviations of multiple experiments. (B) CD spectra showing the changes in helicity of BSA following the addition of MUS-type AuNPs to 1.5 μM BSA at pH 7.4, room temperature (22 °C). Measurements for no-NP control and two NP concentrations are shown.

spacing ranges from 0.7 to 1.0 nm, depending on the core diameter and mixed ligand types and ratio. More detailed information on the surface structure can be found in previous studies.^{17–19}

Stability of the AuNP–Protein Complexes. The change of hydrodynamic diameter (ΔD_h) of the AuNPs following the addition of BSA as monitored by DLS are presented in Figure 1A. The maximum ΔD_h due to BSA adsorption ranged from 5 to 8 nm, depending on the type of AuNPs (Figure S3, Supporting Information). Previous studies also reported a thickness change of 3 nm due to the coating of human serum albumin.²⁴ These ΔD_h suggested that the AuNPs were probably coated with a monolayer of proteins at pH 7.4.

Regarding the difference between different types of AuNPs, the first noticeable difference was the larger ΔD_h for the AuNPs with striped domains (MUS/OT)

compared to AuNPs with all sulfonated alkanethiols (MUS) and AuNPs with randomly distributed MUS and brOT (MUS/brOT). Similarly, for the MPA-type AuNPs, MPA/OT has larger ΔD_h than MPA/brOT (Figure S3, Supporting Information). The different ΔD_h may possibly be due to different BSA affinities (more BSA binding for larger ΔD_h) or different protein geometries on the AuNP surfaces (see the Mode of Interaction section below for further discussion). There is also a difference between the two types of AuNPs, in which the MUS-type has relatively larger ΔD_h than the MPA-type (see the ITC section below for further discussion of the different scenarios).

Following their adsorption onto surfaces, proteins may experience different degrees of conformational change depending on the protein type and surface physicochemical properties (e.g., surface curvature,

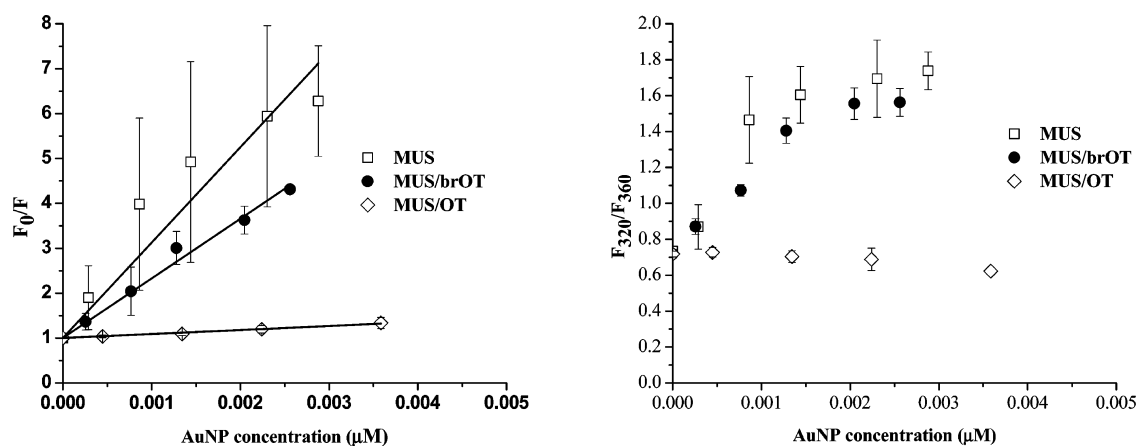


Figure 2. Stern–Volmer plot (left) and the shift of Trp emission (right) for BSA in the presence of increasing concentrations of MUS-type AuNPs. The concentrations of BSA were set to be at $0.15 \mu\text{M}$ in 10 mM 7.4 sodium phosphate buffer with varying amounts of AuNPs added. Experiments were performed at room temperature (22°C). Error bars represent the upper and lower limits of duplicate experiments.

functionality).^{25,26} The degree of conformational change of the adsorbed proteins would influence the resulting properties the AuNP–protein complex. Therefore, to examine whether there was a change in the secondary structure of BSA after adsorption onto different AuNP surfaces, bound and unbound BSA were characterized by CD spectroscopy (Figures 1B and S4, Supporting Information). With a BSA to NP binding ratio of ~ 5 , at least half of the proteins were bound. Although the bound fraction of BSA was significant, the change in the helicity of BSA in the presence of all types of AuNP was small (less than 5% in the helicity at 210 nm). Deconvolution of the CD spectra predicted that BSA without NP addition consisted of 67.4% α -helix and 9.8% β strand (in agreement with Gelamo *et al.*²⁷); these percentages remained the same with the addition of all three types of NPs at two concentrations. These observations suggested that BSA maintained its secondary structure after adsorption onto all types of AuNPs.

Fluorescence Quenching. Fluorescence quenching is a highly sensitive, reproducible, and convenient tool for identifying the binding sites and conformation changes of proteins upon association with small molecules, NPs, and membranes. The efficiency of fluorescence quenching of chromophores in proteins (*e.g.*, tryptophan, tyrosine, and phenylalanine residues) depends on the shielding degree of the chromophores by the quencher, and thus this technique is useful in revealing the relative accessibility of AuNPs to the chromophore groups of protein.^{28,29}

The tryptophan (Trp) residues in BSA were selectively excited herein with an excitation wavelength of 295 nm , at which the competing fluorescence from tyrosine and phenylalanine residues is much weaker. BSA has two Trp residues located in its lower hydrophobic pocket in domain II (Trp-213) and on the surface of the molecule in domain I (Trp-134), respectively.³⁰

Fluorescence emission spectra showed that all tested types of AuNPs quenched the fluorescence of BSA, and the fluorescence intensity decreased gradually with increasing concentration of AuNPs (Figure S5, Supporting Information). More quantitative information can be extracted by fitting the fluorescence quenching data with the Stern–Volmer model.³⁰ The fitting by the Stern–Volmer model to the fluorescence spectra is presented in Figures 2 (left) and 3 (left) and Table 2. The raw fluorescence emission spectra can be found in Figure S5 (Supporting Information).

All k_q values (bimolecular quenching constant) obtained for the three types of AuNPs were at least six orders of magnitude higher than the maximum value ($10^{10} \text{ M}^{-1} \text{ s}^{-1}$) for a diffusion-controlled quenching process. These results suggested that the Trp fluorescence was quenched by specific interactions between BSA and the AuNPs (*i.e.*, static quenching was the dominant mechanism with the formation of bioconjugates). The Stern–Volmer quenching constant (K_{SV}) showed the different quenching ability of the three types of AuNPs. For BSA, the K_{SV} of MUS and MUS/brOT were 2.13×10^9 and $1.33 \times 10^9 \text{ M}^{-1}$, respectively, while it was about an order of magnitude lower ($8.95 \times 10^7 \text{ M}^{-1}$) for MUS/OT. Similarly, between the two MPA-types of AuNPs, MPA/brOT showed higher quenching capability than the striped MPA/OT.

The shifting of emission spectra following the adsorption of BSA on AuNPs was also evaluated by a double wavelength method, in which the ratio of fluorescence intensity at 320 and 360 nm (F_{320}/F_{360}) was registered and plotted against the concentration of AuNPs added (Figures 2 (right) and 3 (right)). As the slope of the ratio showed, F_{320}/F_{360} increased gradually with increasing concentrations of MUS, MUS/brOT and MPA/brOT, while the ratio decreased slightly with increasing concentrations of MUS/OT and MPA/OT. An increasing F_{320}/F_{360} suggests a blue shift of the

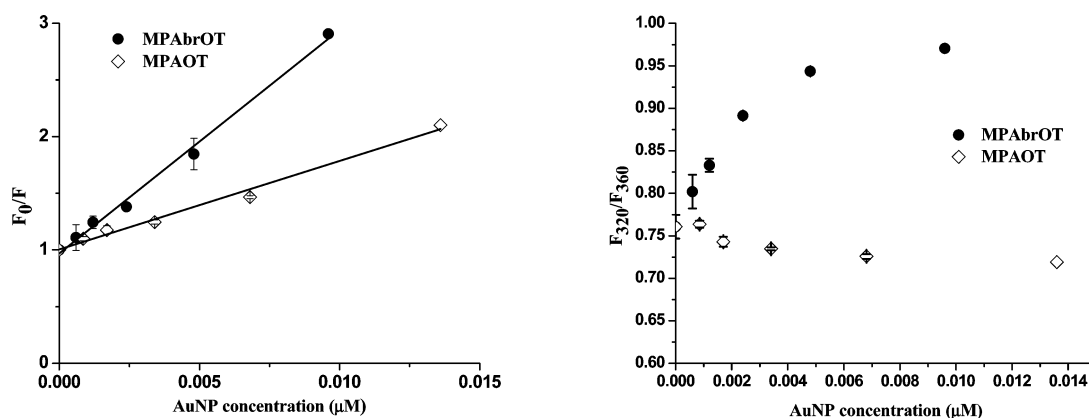


Figure 3. Stern–Volmer plot (left) and the shift of Trp emission (right) for BSA in the presence of increasing concentrations of MPA-type AuNPs. At pH 7.4 and room temperature (22 °C), varying amounts of AuNPs were added to 0.12 μM BSA in 10 mM sodium phosphate buffer. Error bars represent the upper and lower limits of duplicate experiments.

TABLE 2. Fitting Parameters of the Stern–Volmer Model for BSA with Different Particles

types of NPs	MUS	MUS/brOT	MUS/OT	MPA/brOT	MPA/OT
$K_{SV} (\times 10^8 \text{ M}^{-1})$	19.9 ± 3.5	13.6 ± 0.8	0.9 ± 0.1	2.0 ± 0.1	0.8 ± 0.04
$k_q (\times 10^{16} \text{ M}^{-1} \text{ s}^{-1})$	40.0 ± 7.0	27.2 ± 1.5	1.7 ± 0.1	3.9 ± 0.1	1.6 ± 0.08
R^2	0.83	0.98	0.998	0.993	0.986

position of emission maximum that can be considered to be caused by the burying of Trp in a more hydrophobic environment.^{30,31} The slight change of F_{320}/F_{360} in BSA-MUS/OT or MPA/OT indicates less alteration in the Trp environment following adsorption compared to that of MUS, MUS/brOT and MPA/brOT (further discussion of the cause and relevance to the interaction mode can be found below).

It seems conflicting to have larger ΔD_h but lower fluorescence quenching efficiencies for AuNPs with stripe-like domains (MUS/OT or MPA/OT) compared to that of MUS and MUS/brOT or MPA/brOT as observed above. One way to resolve this apparent paradox is to consider the different orientations by which BSA may adsorb onto the AuNPs. Figure 4 is a schematic portraying a possible geometrical arrangement of BSA with respect to the MUS/brOT and MUS/OT particles based on the characterizations presented thus far. These conformations, or ones very similar, would explain the ΔD_h obtained with DLS, the persistence of BSA's secondary structure as measured by CD spectroscopy, and the proximity of the fluorescent Trp residues to the particles shown by the fluorescent quenching experiments. An equilateral triangular prism model has been proposed for BSA, with its side length of 8.4 nm and a thickness of 3.15 nm.^{24,32} When BSA attaches its triangular face onto the surface of the MUS/brOT particles to attain maximum contact, both of the Trp residues will be close to NP surface (<3.15 nm), which will result in an efficient fluorescence quenching and a tight interaction with the NP surface. This may have been the same when BSA adsorbed onto MUS, as it has a homogeneously distributed

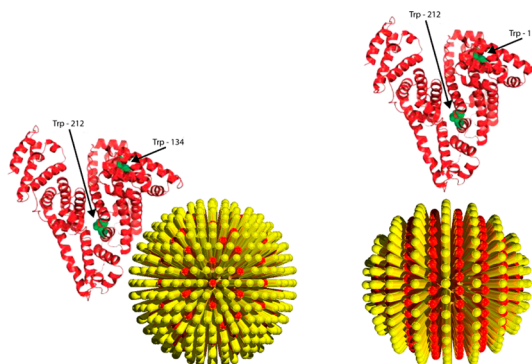


Figure 4. Proposed binding geometries for BSA and (left) MUS/brOT or MPA/brOT and (right) MUS/OT or MPA/OT AuNPs based on DLS and fluorescent quenching measurements. NP and protein size were not drawn to scale (cartoons of AuNP and BSA were adopted and modified from Verma *et al.*¹⁹ and Dubeau *et al.*,³³ respectively).

sulfonated alkanethiols shell. In contrast, if BSA attached onto MUS/OT or MPA/OT with a small contact area that results in the longest dimension being extended into the solution, the two Trp residues will be relatively distant from the NP surface compared to that in the previous configuration. This will result in less shielding of Trp and larger ΔD_h following BSA adsorption. Besides, the extended configuration may also enable MUS/OT or MPA/OT to accommodate more attachment of BSA. Since there are more than one BSA adsorbed onto each NP and they may not adsorb in exactly the same way, Figure 4 only serves as a schematic representation of a possible geometrical arrangement.

ITC and Binding Thermodynamics of NP–Protein Interactions. In this section, we shift from describing the

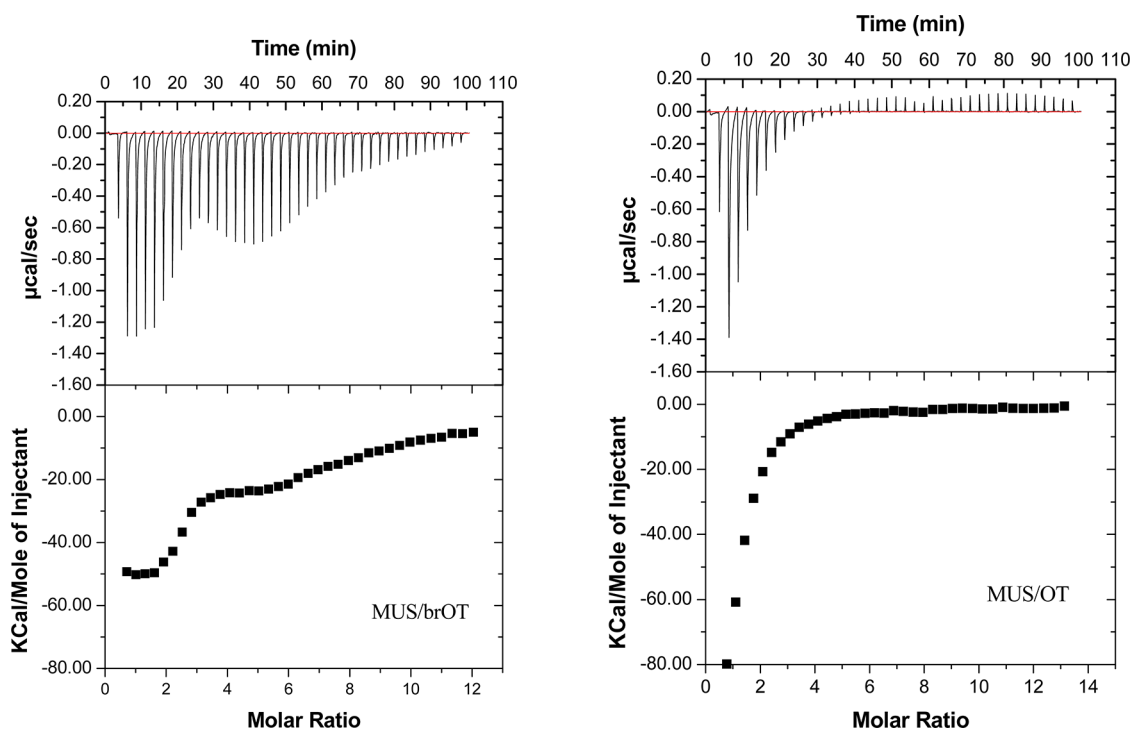


Figure 5. ITC data from the titration of $500\ \mu\text{M}$ BSA into $8.4\ \mu\text{M}$ MUS/brOT and $7.7\ \mu\text{M}$ MUS/OT AuNP. Heat flow versus time during injection of proteins at $25\ ^\circ\text{C}$ and heat evolved per mole of added proteins (corrected for the heat of protein dilution) against the molar ratio (protein/AuNP) for each injection are shown at the top and bottom, respectively. The data corresponding to the heat of dilution of protein are shown in Supporting Information, Figure S7.

geometrical conformation of the proteins to characterizing the binding affinity and thermodynamics of this new orientation.

Protein interaction with particles or surfaces is a complex process that involves various noncovalent forces including Van der Waal force, hydrogen bonding, electrostatic and hydrophobic interactions, the desolvation of both NPs and proteins and solvation of newly formed complexes.³⁴ Depending on the structure of the proteins and the properties of the interacting surface, the relative importance of these various forces will be different. ITC is a useful technique for the characterization of NP–protein interactions as it can directly measure the enthalpy changes and binding stoichiometry between NPs and proteins in solution, from which other thermodynamic quantities such as binding constant, entropy and free energy change can be derived.^{35,36} This quantitative information, in combination with other techniques, can help reveal the mechanisms of the interactions.

As suggested by the aforementioned DLS and fluorescence quenching results, BSA may adopt different orientations when adsorbed onto AuNPs with different surface properties. Accordingly, we expect that there will be observable differences in the ITC heat profiles based on the different modes of interaction between the AuNPs and BSA. As shown by the titration curves (Figures 5 and S7, Supporting Information), the adsorption of BSA onto MUS/OT exhibited a significantly different heat change profile from the other two

types (MUS and MUS/brOT), which have similar heat change profiles. The complexation of BSA with MUS/brOT was consistently exothermic throughout the titration process, while the complexation of BSA with AuNPs with stripe-like domains (MUS/OT) was exothermic only at the beginning (when molar ratio of protein/AuNP is <4). Similarly, the complexation of BSA with MPA/brOT was also consistently exothermic throughout the titration process, and the complexation of BSA with MPA/OT was exothermic at the beginning (when molar ratio of protein/AuNP is <2) and gradually changed to endothermic (Figure 6).

Interestingly, there was a small difference between the MUS-type AuNPs and MPA-type AuNPs. Although the heat profiles were all consistently exothermic, MUS and MUS/brOT showed an abrupt change at a molar ratio of 3, while no such abrupt change was observed for MPA/brOT. Despite the similar trends between MUS/OT and MPA/OT, MPA/OT showed endothermic peaks after the disappearance of exothermic peaks, while no endothermic process was observed for MUS/OT. This difference may have been due to the difference in the curvature and chemistry between the MUS-type and MPA-type AuNPs as the MPA-type particles are 1 nm larger and the charged ligands are carboxyl-terminated instead of sulfonate-terminated. Furthermore, the negatively-charged MPA is shorter than the nonpolar ligands (*i.e.*, OT and brOT) for the MPA-type, while MUS is longer than OT for MUS-type. Adjustment of the initially adsorbed BSA to accommodate

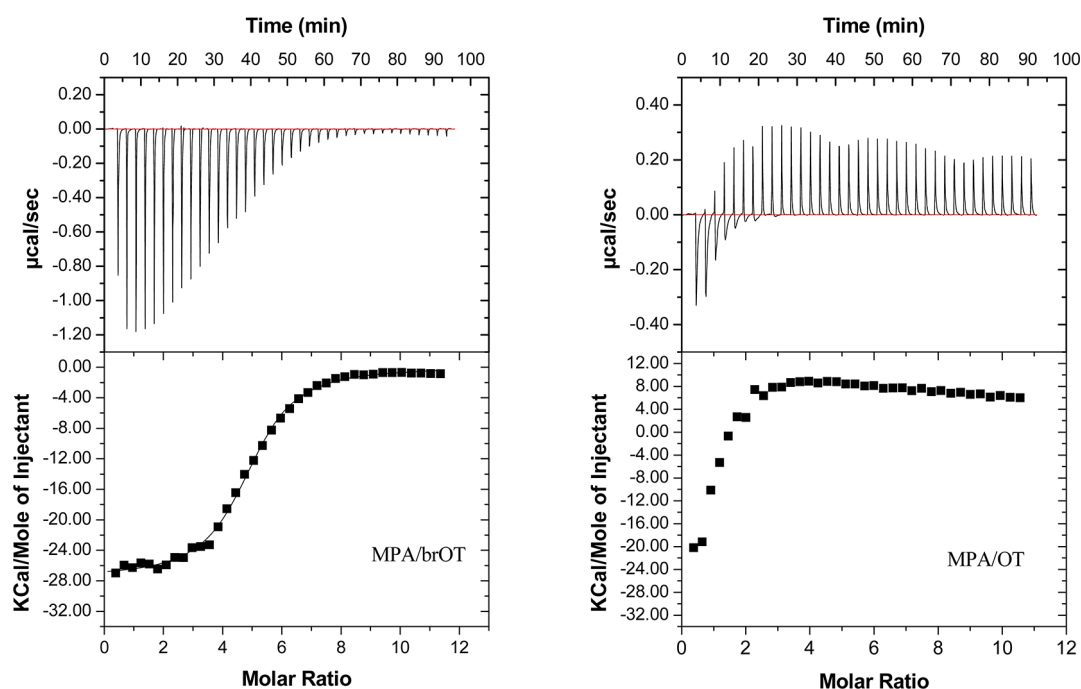


Figure 6. ITC data from the titration of 500 μM BSA into 9.0 μM MPA/brOT (left) and 9.3 μM MPA/OT (right). Heat flow versus time during injection of BSA at 25 $^{\circ}\text{C}$ and heat evolved per mole of added BSA (corrected for the heat of BSA dilution) against the molar ratio (BSA/AuNP) for each injection are shown at the top and bottom, respectively. The data corresponding to the heat of dilution of BSA are shown in Supporting Information, Figure S6.

TABLE 3. Thermodynamic Quantities of BSA and MPA-type NPs Interaction Derived from ITC

NPs	$K_s (\times 10^5 \text{ M}^{-1})$	$-\Delta G (\text{kcal mol}^{-1})$	$\Delta H (\text{kcal mol}^{-1})$	$T\Delta S (\text{kcal mol}^{-1})$	N
MPA-brOT	7.86 ± 0.34	8.03 ± 0.02	-28.10 ± 0.80	-20.07 ± 0.86	4.99 ± 0.15
MPA-OT		heat profile could not be fitted satisfactorily by available models			

subsequent BSA adsorption due to their smaller size may be responsible for the abrupt change in the MUS-type AuNPs, as the heat needed for the disruption of contact would compensate the heat release during new adsorption.

Of all the heat profiles, only the complexation of BSA with MPA/brOT can be satisfactorily fit by available models. It was fit to a model describing a single set of binding sites, and best-fit parameters were calculated using nonlinear least-squares fitting (Table 3). The thermodynamic quantities showed that the adsorption of BSA onto MPA/brOT featured a favorable enthalpy change ($\Delta H < 0$), which was offset partially by an unfavorable entropy loss ($\Delta S < 0$), resulted in an overall negative free energy change ($\Delta G < 0$). Considering that 67% of the ligands were the carboxyl-terminated MPA, the adsorption of BSA onto MPA/brOT was primarily driven by electrostatic interactions, and the binding sites were equivalent for all BSA molecules (since the heat profiles were satisfactorily fitted to a model for the single set of identical binding sites). Besides, a 5:1 binding ratio of BSA to MPA/brOT and a binding constant of $7.86 \times 10^5 \text{ M}^{-1}$ were derived. Despite the small difference between the MUS-type and the MPA-type, the overall similarities in heat profiles and surface

structures suggests that similar electrostatically-driven BSA adsorption was likely to occur on MUS and MUS/brOT.

The overall heat profiles (with a few exothermic peaks at the beginning of titration and some insignificant endothermic peaks later on) observed for MUS/OT and MPA/OT suggested relatively more complex interactions compared to that of the other types of AuNPs. Their overall small heat exchange also indicated that BSA adsorbed onto the NP surface with minimal contact, which seems to be in accordance with the side-on configuration suggested by DLS and fluorescence quenching.

The endothermic adsorption may involve an unfavorable enthalpy contribution ($\Delta H > 0$) and a large favorable entropy change ($\Delta S > 0$) to have a negative free energy of association ($\Delta G < 0$). The positive enthalpy change and favorable entropy change ($\Delta S > 0$) suggested the disruption and release of water from the interaction process,³⁴ which was associated with the adsorption of BSA onto the nonpolar stripes of the AuNPs. Previous studies on these types of AuNPs using molecular dynamic simulation demonstrated that a hydrophobic environment developed over the nonpolar stripes²¹ and that the amphiphilic side chains of

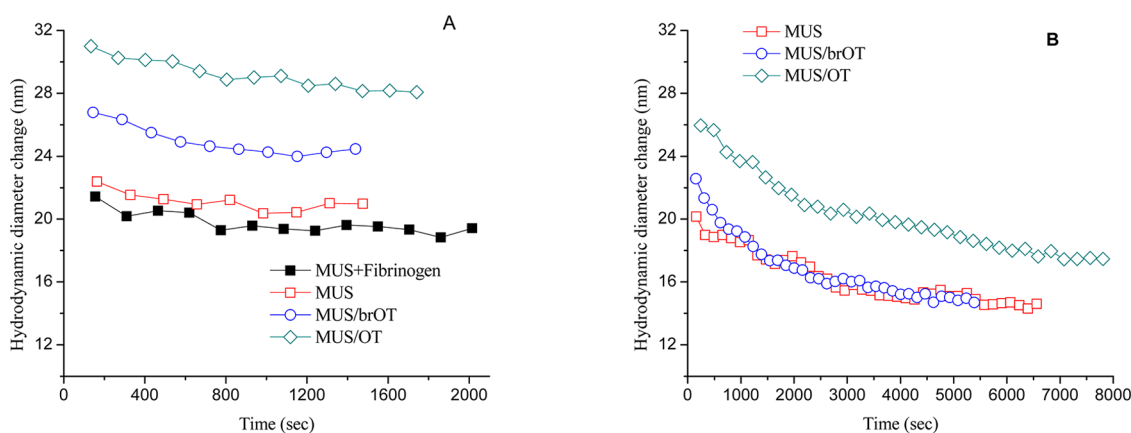


Figure 7. (A) ΔD_h of AuNPs following the addition of a mixture of $0.32 \mu\text{M}$ BSA and $0.32 \mu\text{M}$ fibrinogen, MUS with $0.32 \mu\text{M}$ fibrinogen alone was also shown as a reference; (B) ΔD_h of AuNPs following the further addition of $0.6 \mu\text{M}$ BSA.

lysine and arginine could direct the adsorption of proteins onto the polar and nonpolar ligands.^{21,22}

Interaction with Protein Mixtures. To understand the influence of NP surface heterogeneity in a more complex environment, the interaction between MUS-type AuNPs with a mixture of two proteins was studied by DLS.

The ΔD_h of AuNPs immediately following the addition of 1:1 mixture of BSA and fibrinogen as well as the addition of fibrinogen alone were monitored (Figure 7A; ΔD_h for MUS/brOT and MUS/OT had similar trends, data not shown). The ΔD_h of MUS in the presence of the BSA/fibrinogen mixture was similar to that of fibrinogen alone, while the ΔD_h of MUS/brOT and MUS/OT were larger. These MUS-type AuNPs were found to have a 2:1 binding ratio to fibrinogen.²² Larger ΔD_h for MUS/brOT and MUS/OT may suggest the involvement of BSA in the NP–protein complex with MUS/OT possibly being involving more BSA than MUS/brOT. Further addition of BSA was used to induce an excess of BSA compared to fibrinogen, and the ΔD_h was monitored for 100 min (Figure 7B). Interestingly, the D_h of all AuNP–protein complexes decreased with MUS and MUS/brOT behaving similarly, while the D_h of MUS/OT remained larger than the other two types of AuNPs. The similar ΔD_h for MUS and MUS/brOT further suggested their similar binding affinity with BSA. These observed phenomena indicate that the surface heterogeneity of NPs may still be able to cause a difference in protein adsorption behavior even when there are multiple proteins.

Mode of Interaction. In line with the experimental evidence provided in this study, we propose that the conformation of BSA adsorbing onto NP surfaces depends on the type and form of NP surface heterogeneity.

For particles with stripe-like surface similar to those used in this study, different conformations have been previously proposed for the globular protein cytochrome C and lysozyme in a simulation study based mostly on molecular modeling.^{37,38} In these two studies,

the authors found that the amphiphilic lysine and arginine side chains of Cyt C and lysozyme, respectively, were able to interact simultaneously with polar and nonpolar surface ligands, and particles that exhibited close domains of each type of ligand adsorbed the protein with a varied geometrical conformation.

For the BSA in the present study, the mode of interaction with MUS/OT and MPA/OT may be explained by the same phenomena so that the nonpolar domains in MUS/OT and MPA/OT can help to maintain the nonhydrated regions of the protein. There are positively-charged (arginine- and lysine-rich) surface patches on BSA that serve as electrostatically favorable sites for interaction with the MUS sulfonate ligand headgroup of the AuNPs. Since the $-\text{SO}_3^-$ and $-\text{CH}_3$ terminals on MUS/brOT and MPA/brOT surface are randomly distributed, MUS/brOT and MPA/brOT may behave like particles with a homogeneously charged surface. As such, BSA may not “recognize” the heterogeneity on the surface of MUS/brOT and MPA/brOT and lay its triangular face side on the NP surface to achieve maximal contact. However, due to the nano-scale striations of $-\text{SO}_3^-$ and $-\text{CH}_3$ terminals on the surface of MUS/OT and MPA/OT, the cumulative effects of the nonpolar groups cannot be neglected, as demonstrated by Kuna *et al.*²¹ Therefore, BSA may have to adjust its conformation to fit the surface features on MUS/OT and MPA/OT. The interaction between BSA and MUS/OT or MPA/OT is likely to be a combination of different interactions rather than simple electrostatic interactions as expected in the case of MUS or MUS/brOT or MPA/brOT. It is possible that some BSA approached the stripes of the AuNPs (through electrostatic and/or hydrophobic interactions) with a smaller contact area than that with MUS/brOT, and may lead to longer extension of BSA into solution and loose interactions with the MUS/OT and MPA/OT surfaces. Because of the complex structure of BSA and the dynamic nature of interfacial interactions, detailed information regarding the exact amino acids and side chains in

contact with NPs cannot be obtained with the techniques used in this study.

In spite of their overall similarity in chemical composition, the different experimental results between the MUS/OT (MPA/OT) and MUS/brOT (MPA/brOT) indicated that the structural organization of surface functional groups is no less important than the surface chemistry in protein adsorption. Despite some small differences, the overall similar phenomena observed in both MUS-type and MPA-type AuNPs suggested that the NP surface structure-dependent protein conformation may be generalized regardless of the type of polar ligand used.

It would be worthy to note that characteristics of the adsorbed proteins are also important, as proteins are very diverse in size, shape and surface chemistry. The protein surface is highly heterogeneous and consists of various polar and nonpolar functional groups. All these properties affect the exact nanoscale physicochemical identities of the protein surface that interacts with the available sites on NP surface. For example, the size and shape of proteins were found to determine the binding stoichiometry for the same types of NPs.³⁶ In a study by Hung *et al.*, they also stressed the importance of the structural characteristics of the particular protein under examination for the prevalence of the conformational change of the protein upon adsorption to structured surfaces.³⁷ In our study, the surface heterogeneity of BSA allows the protein to adopt different conformations to adsorb onto AuNPs exhibiting nanoscale surface heterogeneities. In the case of MUS and MUS/brOT, sites on the BSA surface with more positively-charged side chains are likely to interact with the negatively-charged ligands on the NP surface, while sites with more nonpolar side chains may come in direct contact with the nonpolar stripes on MUS/OT NPs. Delicate control by the chemical heterogeneity (surface charge distribution) of proteins was illustrated by Treuel *et al.* (2014),³⁹ in which human serum albumin with different modifications were

shown to adopt different orientations on NP surfaces. However, in our study, it is the surface heterogeneity of NPs that determines the orientations of the adsorbed proteins, and the heterogeneous surface of the interacting proteins makes this control possible.

These surface structure-determining protein coatings have important implications: (1) the surface heterogeneity of NPs can be manipulated to selectively adsorb proteins in relevant systems; (2) organization of the adsorbed proteins may affect their activity, as demonstrated by the esterase activity results that showed that BSA retained higher esterase activity in the presence of MPA/OT than that of MPA/brOT (Figure S7, Supporting Information). Overall, this study demonstrated the potential of using surface structural heterogeneity as a new tunable property in the design of NPs to modulate the conformation of adsorbed molecules. Further studies are needed to investigate the behavior of these AuNPs with different ligand conformations in more biologically relevant systems.

CONCLUSION

In summary, the adsorption of BSA onto three MUS-type and two MPA-type AuNPs was studied using a combination of DLS, CD spectroscopy, fluorescence quenching, and ITC. The results showed different protein adsorption behaviors depending on the NP surface ligand composition and structure. BSA adsorption onto particles with nanoscale stripe-like polar and nonpolar domains behaved differently from AuNPs with randomly distributed mixed terminals and homogeneously charged terminals. The different binding modes affected protein configuration and interaction affinity. Results suggested that the surface structural and chemical heterogeneity of NPs is important in determining the protein–NP surface interaction and subsequent protein conformation. This study also demonstrated that NP surface heterogeneity could be a tunable property in NP design for specific applications.

METHODS

Preparation of AuNPs and Protein Suspension. The synthesis of SAM-coated AuNPs with diverse surface composition and structures can be found in previous studies^{14,17,18} and in the Supporting Information. To prepare the stock suspensions of AuNPs, the AuNP powder was added into either ultrapure water (Millipore Simplicity, >18 M Ω -cm) or dialyzed sodium phosphate solution. The suspensions were sonicated in an ultrasonic bath (VWR, B2500A-MT) for 30 min. After ultrasonication, the AuNP suspensions were centrifuged at 9000 rpm for 15 min (Eppendorf 5417c centrifuge) to remove nondispersive aggregates from the suspensions. The mass concentration was determined using a PerkinElmer ELAN 9000 inductively-coupled plasma mass spectrometer (ICP-MS) (Waltham, MA), which was then converted to molar concentration based on the NP geometry characterized by TEM (mass of single AuNP was calculated based on its density and average core size).

Bovine serum albumin (BSA, lyophilized powder, \geq 98%) was purchased from Sigma and used without further purification.

The stock solution of the proteins was prepared in 10 mM sodium phosphate buffer solution (PBS) of pH 7.4 and stored at 4 °C, and the stock solution was used within 1 week. Buffers at pH 7.4 were prepared using 10 mM sodium phosphate buffer solution.

Dynamic Light Scattering. The hydrodynamic diameter of AuNPs was measured using a Malvern Zetasizer Nano ZS (Worcestershire, U.K.) with a fixed detector angle of 173°. Specifically, at pH 7.4, the AuNP stock suspension (\sim 0.05 μ M) was sequentially added with protein stock solution to reach a series of final protein/AuNP molar ratios that ranged from 1 to 20. The mixture was incubated for 30 min before DLS measurement, and a total of 15 measurements were taken. At least duplicate experiments were performed for each data point.

Circular Dichroism Spectroscopy. CD measurements were undertaken by a Jasco J-810 spectropolarimeter (Easton, MD) with a 2 mm path length rectangular quartz cell at room temperature (22 °C). The CD spectra were recorded from 190 to 260 nm, and each spectrum was an average of 5 scans. The concentration of BSA was fixed (1.5 μ M), and the AuNPs concentration varied

from 0 to 0.2 μM . The CD spectra were deconvoluted to obtain their α helix and β strand content using an online algorithm K2D3 (<http://k2d3.org.ca/>).

Fluorescence Quenching Measurements. Fluorescence measurements were performed on a HITACHI F-7000 fluorescence spectrophotometer (Tokyo, Japan) with the use of a 1.00 cm path length rectangular quartz cell. The spectra were recorded in the wavelength range of 310–500 nm upon excitation at 295 nm, using 10 nm/10 nm slit widths, and each spectrum was an average of two scans. The concentrations of BSA were set to be at 0.15 μM (for MUS-type) and 0.12 μM (for MPA-type), and the concentration of AuNPs ranged from 0 to 0.004 μM for MUS-type AuNPs, 0 to 0.014 μM for MPA-type AuNPs. Blanks corresponding to the buffer were subtracted from the sample spectra to correct the fluorescence background before performing the analysis. Duplicate experiments were conducted for each AuNP concentration.

Since the AuNP concentrations were relatively low, where fluorescence quenching was dominated by diffusive transport, a nonequilibrium model for the fluorescence quenching is considered to be more appropriate.^{28,30} The Stern–Volmer model, which predicts the ratio F_0/F at low concentrations of quenching agents to be linear, is the standard model for this regime. Thus, it was being used to analyze the fluorescence intensity data.

$$\frac{F_0}{F} = 1 + k_q\tau_0[\text{AuNP}] = 1 + K_{SV}[\text{AuNP}]$$

where F_0 and F are the maximum fluorescence intensities in the absence and presence of AuNP, respectively, k_q is the quenching constant, τ_0 is the lifetime of the fluorophore in the absence of quencher, K_{SV} is the Stern–Volmer fluorescence quenching constant, which is a measure of the quenching efficiency, and $[\text{AuNP}]$ is the quencher concentration.

Isothermal Titration Calorimetry. ITC measurements were performed on a MicroCal ITC200 system (GE Healthcare). BSA was dialyzed overnight against 10 mM sodium phosphate buffer (renewed three times), and the AuNPs were dissolved in the last dialysate (sonicated, then centrifuged at 9000 rpm for 15 min). A typical titration experiment involved 38 injections of BSA (titrant, 1 μL per injection from a 500 μM stock) at 150 sec intervals into the sample cell (volume = 200 μL) containing the AuNPs solution (MUS, 7.03 μM ; MUS/brOT, 8.43 μM ; MUS/OT, 7.73 μM ; MPA/brOT, 8.95 μM ; MPA/OT, 9.3 μM). The reference cell was filled with 10 mM sodium phosphate buffer. During the experiment, the sample cell was stirred continuously at 1000 rpm.

The heat of BSA dilution in the buffer alone was subtracted from the titration data (both normalized to 0) for each experiment. The data were analyzed to determine the binding stoichiometry (N), affinity constant (K_d), and other thermodynamic parameters of the reaction using the coupled Origin software. The reported thermodynamic parameters were an average of duplicate experiments.

Conflict of Interest: The authors declare no competing financial interest.

Acknowledgment. The authors would like to thank C. Moehnke for his assistance in using various spectroscopy instruments and the Molecular Biosciences Center of Baylor University for the use of centrifuge. We are grateful to M. Trawick for the opportunity and access to the MicroCal ITC200 system. RPC and FS would like to acknowledge the Swiss National Foundation NRP 64 program for supporting this work.

Supporting Information Available: Text and figures describing particle synthesis and characterization of interactions. This material is available free of charge via the Internet at <http://pubs.acs.org>.

REFERENCES AND NOTES

1. Koegler, P.; Clayton, A.; Thissen, H.; Santos, G. N. C.; Kingshott, P. The Influence of Nanostructured Materials on Biointerfacial Interactions. *Adv. Drug Delivery Rev.* **2012**, *64*, 1820–1839.

2. Nel, A. E.; Madler, L.; Velegol, D.; Xia, T.; Hoek, E. M. V.; Somasundaran, P.; Klaessig, F.; Castranova, V.; Thompson, M. Understanding Biophysicochemical Interactions at the Nano-Biointerface. *Nat. Mater.* **2009**, *8*, 543–557.
3. Lynch, I.; Cedervall, T.; Lundqvist, M.; Cabaleiro-Lago, C.; Linse, S.; Dawson, K. A. The Nanoparticle–Protein Complex as a Biological Entity; A Complex Fluids and Surface Science Challenge for the 21st Century. *Adv. Colloid Interface Sci.* **2007**, *134–135*, 167–174.
4. Rana, S.; Yeh, Y. C.; Rotello, V. M. Engineering the Nanoparticle–Protein Interface: Applications and Possibilities. *Curr. Opin. Chem. Biol.* **2010**, *14*, 828–834.
5. Monopoli, M. P.; Aberg, C.; Salvati, A.; Dawson, K. A. Biomolecular Coronas Provide the Biological Identity of Nanosized Materials. *Nat. Nanotechnol.* **2012**, *7*, 779–786.
6. Lundqvist, M.; Stigler, J.; Elia, G.; Lynch, I.; Cedervall, T.; Dawson, K. A. Nanoparticle Size and Surface Properties Determine the Protein Corona with Possible Implications for Biological Impacts. *Proc. Natl. Acad. Sci. U. S. A.* **2008**, *105*, 14265–14270.
7. Chakraborty, S.; Joshi, P.; Shanker, V.; Ansari, Z. A.; Singh, S. P.; Chakrabarti, P. Contrasting Effect of Gold Nanoparticles and Nanorods with Different Surface Modifications on the Structure and Activity of Bovine Serum Albumin. *Langmuir* **2011**, *27*, 7722–7731.
8. Meder, F.; Daberkow, T.; Treccani, L.; Wilhelm, M.; Schowalter, M.; Rosenauer, A.; Madler, L.; Rezwani, K. Protein Adsorption on Colloidal Alumina Particles Functionalized with Amino, Carboxyl, Sulfonate and Phosphate Groups. *Acta Biomater.* **2012**, *8*, 1221–1229.
9. Chen, K.; Xu, Y.; Rana, S.; Miranda, O. R.; Dubin, P. L.; Rotello, V. M.; Sun, L.; Guo, X. Electrostatic Selectivity in Protein–Nanoparticle Interactions. *Biomacromolecules* **2011**, *12*, 2552–2561.
10. Cedervall, T.; Lynch, I.; Lindman, S.; Berggård, T.; Thulin, E.; Nilsson, H.; Dawson, K. A.; Linse, S. Understanding the Nanoparticle–Protein Corona Using Methods to Quantify Exchange Rates and Affinities of Proteins for Nanoparticles. *Proc. Natl. Acad. Sci. U. S. A.* **2007**, *104*, 2050–2055.
11. Walczyk, D.; Bombelli, F. B.; Monopoli, M. P.; Lynch, I.; Dawson, K. A. What the Cell “Sees” in Bionanoscience. *J. Am. Chem. Soc.* **2010**, *132*, 5761–5768.
12. Lundqvist, M.; Stigler, J.; Cedervall, T.; Berggård, T.; Flanagan, M. B.; Lynch, I.; Elia, G.; Dawson, K. The Evolution of the Protein Corona Around Nanoparticles: A Test Study. *ACS Nano* **2011**, *5*, 7503–7509.
13. Gagner, J. E.; Shrivastava, S.; Qian, X.; Dordick, J. S.; Siegel, R. W. Engineering Nanomaterials for Biomedical Applications Requires Understanding the Nano-Bio Interface: A Perspective. *J. Phys. Chem. Lett.* **2012**, *3*, 3149–3158.
14. Jackson, A. M.; Myerson, J. W.; Stellacci, F. Spontaneous Assembly of Subnanometre-Ordered Domains in the Ligand Shell of Monolayer-Protected Nanoparticles. *Nat. Mater.* **2004**, *3*, 330–336.
15. Hodgkinson, G.; Hlady, V. Relating Material Surface Heterogeneity to Protein Adsorption: the Effect of Annealing of Micro-Contact-Printed OTS Patterns. *J. Adhes. Sci. Technol.* **2005**, *19*, 235–255.
16. Ta, T. C.; McDermott, M. T. Mapping Interfacial Chemistry Induced Variations in Protein Adsorption with Scanning Force Microscopy. *Anal. Chem.* **2000**, *72*, 2627–2634.
17. Uzun, O.; Hu, Y.; Verma, A.; Chen, S.; Centrone, A.; Stellacci, F. Water-Soluble Amphiphilic Gold Nanoparticles with Structured Ligand Shells. *Chem. Commun.* **2008**, 196–198.
18. Jackson, A. M.; Hu, Y.; Silva, P. J.; Stellacci, F. From Homoligand- to Mixed-Ligand-Monolayer-Protected Metal Nanoparticles: A Scanning Tunneling Microscopy Investigation. *J. Am. Chem. Soc.* **2006**, *128*, 11135–11149.
19. Verma, A.; Uzun, O.; Hu, Y. H.; Hu, Y.; Han, H. S.; Watson, N.; Chen, S. L.; Irvine, D. J.; Stellacci, F. Surface-Structure-Regulated Cell-Membrane Penetration by Monolayer-Protected Nanoparticles. *Nat. Mater.* **2008**, *7*, 588–595.
20. Centrone, A.; Penzo, E.; Sharma, M.; Myerson, J. W.; Jackson, A. M.; Marzari, N.; Stellacci, F. The Role of Nanostructure in the Wetting Behavior of Mixed-Monolayer-Protected

- Metal Nanoparticles. *Proc. Natl. Acad. Sci. U. S. A.* **2008**, *105*, 9886–9891.
21. Kuna, J. J.; Voitchovsky, K.; Singh, C.; Jiang, H.; Mwenifumbo, S.; Ghorai, P. K.; Stevens, M. M.; Glotzer, S. C.; Stellacci, F. The Effect of Nanometre-Scale Structure on Interfacial Energy. *Nat. Mater.* **2009**, *8*, 837–842.
 22. Huang, R.; Carney, R. P.; Stellacci, F.; Lau, B. L. T. Protein–NanoParticle Interactions: the Effects of Surface Compositional and Structural Heterogeneity are Scale Dependent. *Nanoscale* **2013**, *5*, 6928–6935.
 23. Liu, X.; Yu, M.; Kim, H.; Mameli, M.; Stellacci, F. Determination of Monolayer-Protected Gold Nanoparticle Ligand–Shell Morphology Using NMR. *Nat. Commun.* **2012**, *3*, 1182.
 24. Rocker, C.; Potzl, M.; Zhang, F.; Parak, W. J.; Nienhaus, G. U. A Quantitative Fluorescence Study of Protein Monolayer Formation on Colloidal Nanoparticles. *Nat. Nano.* **2009**, *4*, 577–580.
 25. Roach, P.; Farrar, D.; Perry, C. C. Interpretation of Protein Adsorption: Surface-Induced Conformational Changes. *J. Am. Chem. Soc.* **2005**, *127*, 8168–8173.
 26. Lundqvist, M.; Sethson, I.; Jonsson, B. H. Protein Adsorption onto Silica Nanoparticles: Conformational Changes Depend on the Particles' Curvature and the Protein Stability. *Langmuir* **2004**, *20*, 10639–10647.
 27. Gelamo, E. L.; Silva, C. H. T. P.; Imasato, H.; Tabak, M. Interaction of Bovine (BSA) and Human (HSA) Serum Albumins with Ionic Surfactants: Spectroscopy and Modelling. *Biochim. Biophys. Acta, Protein Struct. Mol. Enzymol.* **2002**, *1594*, 84–99.
 28. Lacerda, S. H. D.; Park, J. J.; Meuse, C.; Pristiniski, D.; Becker, M. L.; Karim, A.; Douglas, J. F. Interaction of Gold Nanoparticles with Common Human Blood Proteins. *ACS Nano* **2010**, *4*, 365–379.
 29. Sandros, M. G.; Gao, D.; Gokdemir, C.; Benson, D. E. General, High-Affinity Approach for the Synthesis of Fluorophore Appended Protein Nanoparticle Assemblies. *Chem. Commun.* **2005**, 2832–2834.
 30. Dong, S. J.; Shang, L.; Wang, Y. Z.; Jiang, J. G. pH-Dependent Protein Conformational Changes in Albumin: Gold Nanoparticle Bioconjugates: A Spectroscopic Study. *Langmuir* **2007**, *23*, 2714–2721.
 31. Cukalevski, R.; Lundqvist, M.; Oslakovic, C.; Dahlback, B.; Linse, S.; Cedervall, T. Structural Changes in Apolipoproteins Bound to Nanoparticles. *Langmuir* **2011**, *27*, 14360–14369.
 32. Ferrer, M. L.; Duchowicz, R.; Carrasco, B.; de la Torre, J. G.; Acuna, A. U. The Conformation of Serum Albumin in Solution: A Combined Phosphorescence Depolarization-Hydrodynamic Modeling Study. *Biophys. J.* **2001**, *80*, 2422–2430.
 33. Dubeau, S.; Bourassa, P.; Thomas, T. J.; Tajmir-Riahi, H. A. Biogenic and Synthetic Polyamines Bind Bovine Serum Albumin. *Biomacromolecules* **2010**, *11*, 1507–1515.
 34. De, M.; You, C.-C.; Srivastava, S.; Rotello, V. M. Biomimetic Interactions of Proteins with Functionalized Nanoparticles: A Thermodynamic Study. *J. Am. Chem. Soc.* **2007**, *129*, 10747–10753.
 35. Lindman, S.; Lynch, I.; Thulin, E.; Nilsson, H.; Dawson, K. A.; Linse, S. Systematic Investigation of the Thermodynamics of HSA adsorption to *N*-iso-propylacrylamide/*N*-tert-butylacrylamide copolymer nanoparticles. Effects of particle size and hydrophobicity. *Nano Lett.* **2007**, *7*, 914–920.
 36. De, M.; Miranda, O. R.; Rana, S.; Rotello, V. M. Size and Geometry Dependent Protein–Nanoparticle Self-assembly. *Chem. Commun.* **2009**, 2157–2159.
 37. Hung, A.; Mwenifumbo, S.; Mager, M.; Kuna, J. J.; Stellacci, F.; Yarovsky, I.; Stevens, M. M. Ordering Surfaces on the Nanoscale: Implications for Protein Adsorption. *J. Am. Chem. Soc.* **2011**, *133*, 1438–1450.
 38. Hung, A.; Mager, M.; Hembury, M.; Stellacci, F.; Stevens, M. M.; Yarovsky, I. Amphiphilic Amino Acids: a Key to Adsorbing Proteins to Nanopatterned Surfaces? *Chem. Sci.* **2013**, *4*, 928–937.
 39. Treuel, L.; Brandholt, S.; Maffre, P.; Wiegele, S.; Shang, L.; Nienhaus, G. U. Impact of Protein Modification on the Protein Corona on Nanoparticles and Nanoparticle–Cell Interactions. *ACS Nano* **2013**, *8*, 503–513.